TMS 2017

146th Annual Meeting & Exhibition

SUPPLEMENTAL PROCEEDINGS

TMS

Springer

The Use of Laser Ultrasound to Detect Defects in Laser Melted Parts

Sarah Everton, Phill Dickens, Chris Tuck, Ben Dutton and David Wimpenny

Abstract Additive manufacturing (AM) offers a number of benefits over conventional manufacturing, giving an increased design freedom and the opportunity to integrate multiple components, saving weight. The rigorous standard for material integrity set by the Aerospace sector necessitates the development of systems to ensure quality. Laser ultrasonic testing (LU) is a non-contact inspection technique which has been proposed as suitable for in-situ monitoring of additive manufacturing processes, as measurements can be taken at elevated temperatures. This paper will show the capability of this technique for assuring material quality in metal AM parts and compare LU with x-ray computed tomography (XCT).

Keywords Laser ultrasound · Defect characterisation · Non-destructive testing · Additive manufacturing · Laser powder bed fusion

Introduction

The development of additive manufacturing (AM) processes in recent years, due in-part to an increased understanding of key process variables (KPVs), materials and the underlying design principles, has resulted in a rapid uptake of the technology across multiple engineering sectors [1]. With AM offering the opportunity to save on product weight and cost, simplify assemblies and enhance component performance, it is the lack of assurance of AM part quality proving a key barrier for the Aerospace sector [2].

S. Everton · P. Dickens (✉) · C. Tuck
Additive Manufacturing and 3D Printing Research Group, University of Nottingham, University Park, Nottingham NG7 2RD, UK
e-mail: phill.dickens@nottingham.ac.uk

S. Everton · B. Dutton · D. Wimpenny
The Manufacturing Technology Centre, Ansty Business Park, Pilot Way, Coventry, Warwickshire CV7 9JU, UK

The Minerals, Metals & Materials Society, *TMS 2017 146th Annual Meeting & Exhibition Supplemental Proceedings*, The Minerals, Metals & Materials Series,
DOI 10.1007/978-3-319-51493-2_11

The in-situ acquisition of data through process monitoring has been identified as a priority area of research by the US National Institute of Standards and Technology [3] and the UK AM Steering Group [4]. The in-situ detection of defects and use of closed-loop process control will increase AM process robustness and remove the barrier to adoption of AM, for Aerospace. The term AM refers to a number of different processes, characterised by the energy source, feedstock or melting mechanism. A comprehensive introduction to AM is given by Gibson et al. [5]. This paper focusses on the identification of defects generated during manufacturing by laser powder bed fusion (PBF).

Laser PBF has a large number of input parameters which affect the quality of the final component build [6] and therefore, many studies have been carried out to assess the effects of these, sometimes interdependent, parameters [7, 8]. Commonly occurring "defects" include material discontinuities such as pores, inclusions and cracks. Limiting the porosity of AM components is essential to avoid adversely affecting a components material performance [9]. Several different mechanisms are responsible for the generation of pores during laser PBF processing, yielding pores with different characteristics. Selecting parameter combinations that result in over- or under-melting of the material results in increased porosity. The pores can be further distinguished by their shape and can be categorised as spherical [10], keyhole [11] or elongated pores [12]. The different pores vary in size from spherical pores with 20 μm diameter to elongated pores in the region of 500 μm length, sometimes longer.

In time, as understanding of the formation mechanisms and the relationship between input parameters is developed, these defect will be largely eradicated. However, in order to aid this development and to enable the use of AM components where quality assurance is needed, in-situ monitoring can be employed. Many non-destructive monitoring methods have been trialled such as thermographic and visual monitoring systems [13], but these systems are limited to the identification of surface defects. Surface defects can be healed as the subsequent layers are processed so to avoid false positives, inspection systems that allow for identification of sub-surface defects are recommended.

Laser ultrasound (LU) is a good candidate for in-situ inspection of sub-surface defects, as the technique can be utilised on "rough" AM surfaces eliminating the coupling problems associated with conventional ultrasonic methods and can operate at high temperatures. Only a handful of experiments have been carried out to date trialling LU for inspection of AM surfaces [14–16] although capability of detecting AM type defects is more widely studied [17, 18]. Prior to being implemented in-situ, the capability of LU for detection of sub-surface AM defects must be proven, ex situ.

In this study, LU has been used to give material quality assurance for Ti-6Al-4 V AM samples, ex situ. Sample integrity has also been investigated using XCT and validated by destructive testing.

Laser Ultrasound

Background

To generate ultrasonic waves, a pulsed generation laser is directed at the sample surface. In high energy mode, termed the ablative mode, a region of plasma is formed directly above the impact point. When the energy build up is sufficient, the plasma expands and is ejected from the sample surface. The recoil force from this ejection generates an ultrasonic wave which travels into the sample and along the sample surface.

There are several types of ultrasonic waves generated, which are categorised based on their mode of propagation. "Surface" or near-to-surface waves travel along the surface of a sample. A Rayleigh wave is a type of surface wave which propagates with elliptical orbit and can penetrate into a sample approximately the same distance as its wavelength. In this experiment, a pulsed laser with a wavelength of 1064 nm was utilised, so the expected penetration is also in the region of 1064 nm. "Bulk" waves are so named because they penetrate into the bulk of the material from the generation source. These waves will travel until they meet an interface such as the wall, or base of the sample. When a boundary is encountered, the waves can reflect or propagate and energy can be transferred between wave types, termed mode conversion. The two main bulk wave types are longitudinal waves which travel by compression, or transverse waves which have displacements perpendicular to the direction of penetration (also termed Shear waves).

In LU, a laser is also used at the detection point, a fixed distance from the generation laser, to identify surface displacements caused by the arrival of the ultrasonic wave types. An interferometer splits the continuous wavelength laser beam into a reference beam and a beam which is directed at the sample surface. In a fully dense sample, with no defects present, the incident generated and reflected waves arrive at the detection point after an elapsed time. The velocity of each wave type in elastic solids is different, so displacement of the surface over time can be attributed to the arrival of each wave type. The interferometer gives two readings at each point, over the selected time period, an alternating current (AC) and a direct current (DC) reading. The DC monitor gives a signal that is proportional to the power of the signal beam on the detector and gives a measure of the light reflected from the surface. The AC signal output delivers the AC voltage corresponding to the instantaneous out of plane surface displacement at that point, for ultrasonic frequencies. At positions of low light (low DC), the AC signal amplitude will also be low. Dividing through the AC signal by the mean DC value normalises this effect. The compensated AC signal can then be displayed visually for analysis.

If a sub-surface defect is present between the two LU lasers, the tips of defect act as a diffraction source and the detection laser receives diffracted Rayleigh wave signals from the defect, along with direct waves and bulk waves which have bounced back from the side and end walls, or the bottom of the sample.

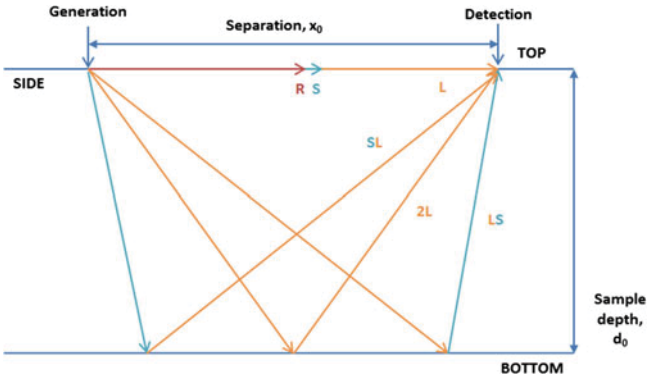

Fig. 1 Schematic showing approximate paths of direct, reflected and mode conversed ultrasonic waves

Fig. 2 A typical A-scan, extracted from LaserScan with surface displacements from wave arrivals indicated, for a defect-free sample

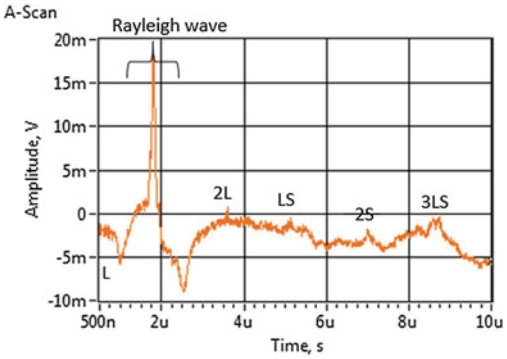

Interrogation of the resulting data in the time-window of the Rayleigh wave arrival will give indication of whether or not defects are present.

Figure 1 shows a schematic of the wave paths for direct longitudinal (L) and shear (S) bulk waves and reflected bulk waves (2L). Mode converted waves reflecting off the bottom interface (LS, SL) are also shown. The surface Rayleigh (R) wave also passes directly between the generation and detection lasers at separation, $x_{o.}$

Ultrasonic data is typically displayed in two ways: firstly, an A-scan is produced at each scanning location, which displays the received ultrasonic energy at the detection point, as a function of time (Fig. 2). The Rayleigh wave's comparatively large amplitude makes it easier to analyse.

Secondly, a motorised stage is used to move the lasers along and a snapshot is taken at defined distance intervals along the top of the sample. The series of A-scans are then compiled and stacked to create a profile view of the sample, termed a B-scan (Fig. 3). The expected arrival times for each wave and mode-converted wave type are overlaid. The diagonal lines that can be seen are

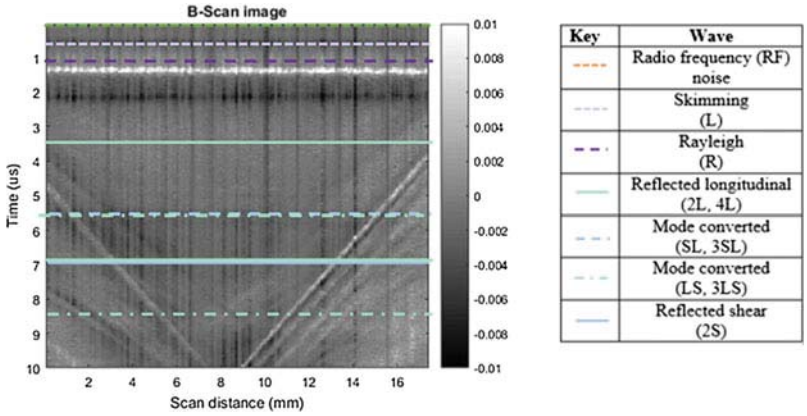

Fig. 3 Predicted wave arrival times overlaid on a B-scan for a defect-free sample, with key

reflections from the end walls of the sample, as the laser unit moves farther from one end, the time for the wave to travel to the detection point increases. Similarly, the laser unit moves towards the other end of the sample and the wave travel time decreases.

As the lasers traverse along a sample surface at a fixed separation distance, if a defect is present, any interaction of the Rayleigh wave with the defect shows as a parabolic indication.

Experimental Set-up

The laser ultrasonic testing system uses a pulsed laser (class IV, Q-switched Nd: YAG laser with a wavelength of 1064 nm, capable of delivering 200 mJ energy with each 10 ns pulse at 20 Hz frequency) to generate ultrasonic waves in a sample and a continuous wave detection laser (10 W, 1550 nm ± 10 nm wavelength fibre laser), interferometer, oscilloscope and computer.

The Ti6Al4V cubes were built using a Renishaw AM250 at a power of 200 W, 600 mm/s scanning speed at 150 μm hatch spacing. The build pattern was rotated by an angle increment of 67° at each 40 μm layer. The larger cubes were sliced into 10 × 10 × 30 mm blocks and through-holes with various diameters were manufactured by EDM at a variety of depths. The top surface was left in the as-built condition (Fig. 4).

The LU system was set up such that in-line measurements were taken along the x-direction of the sample, with the generation laser line following the detection laser spot along the length of the sample. The sample was mounted on a motorised stage so that the sample could be moved in the y-direction to examine alternative scanning lines, without the need to relocate the sample (Fig. 5).

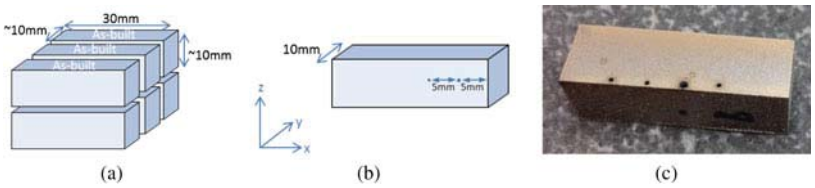

Fig. 4 Schematic showing **a** slicing pattern and block size, **b** targeted hole spacing and **c** a photograph of the sample block

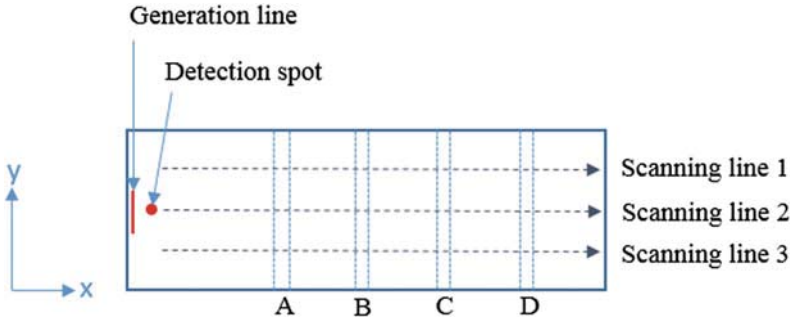

Fig. 5 Schematic showing laser starting positions, the four hole positions and the three laser scanning lines

A laser spacing of 3 mm was calculated as necessary to avoid interference of the reflected bulk waves with the surface wave arrival. The signal was measured over 10 μs at each acquisition point and the average of 64 shots recorded. The LU data generated in LaserScan software was exported for signal processing and analysis in Matlab.

Results

LU

The samples were scanned along three scanning lines indicated in Fig. 5 and a B-scan generated for each dataset (Figs. 6, 7 and 8). The data has been processed to eliminate the laser shot noise, reduce background noise and to remove the DC offset, then scaled by the maximum signal amplitude to allow a direct comparison between B-scans to be made.

The four large through-holes are indicated by four ‘triangles’ in the above B-scans, peaking at roughly 7, 12, 17 and 22 mm scan distance. The reflected and mode-converted waves appear as “trails” after the arrival of the Rayleigh wave

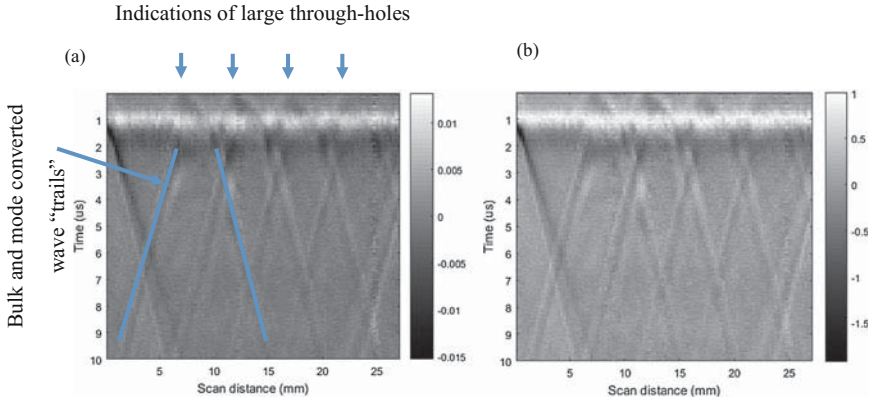

Fig. 6 Scanning line 1 B-scans showing amplitude variation (mV) and elapsed time **a** filtered and **b** filtered and scaled

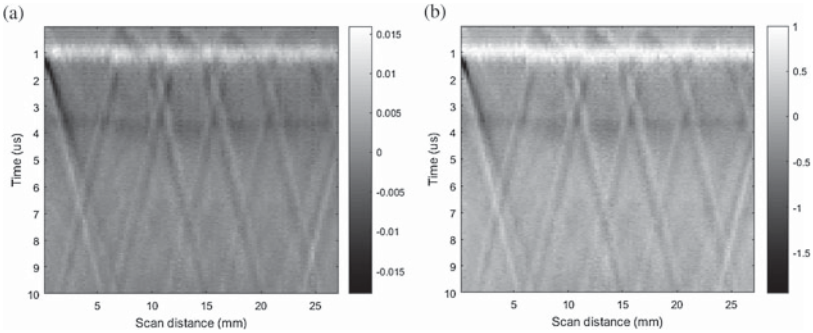

Fig. 7 Scanning line 2 B-scans showing amplitude variation (mV) and elapsed time **a** filtered and **b** filtered and scaled

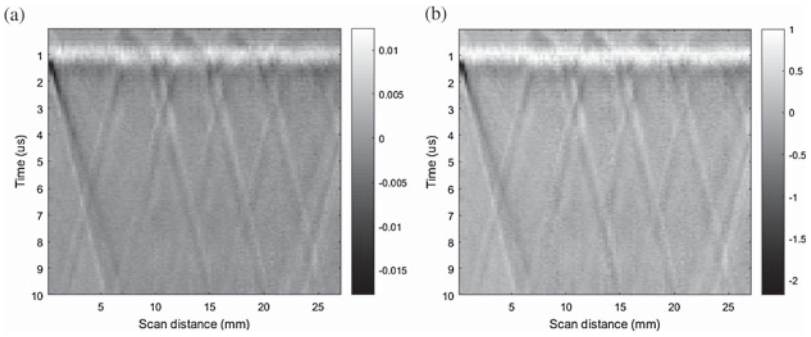

Fig. 8 Scanning line 3 B-scans showing amplitude variation (mV) and elapsed time **a** filtered and **b** filtered and scaled

which arrives at approximately 1 μs. No further defects are indicated. The B-scans generated from different scanning lines can be directly compared, highlighting any changes in wave arrival times. Very small changes are seen in the arrival time of the Rayleigh and reflected shear waves from scan to scan; this is thought to be due to the geometry of the sample.

If the top surface and bottom surface were not cut parallel the laser spacing would be altered when moving between channels. Similarly, if the samples were not a uniform thickness across the y-direction and thus, the reflected bulk wave arrival times would be different, as is the case here. Differences in wave arrival times seen in the "trail" sections are indicative of a variation in hole depth across the channels (y-direction). This was validated using focus variation microscopy (FVM) to measure the hole exit and entry locations. Due to the manufacturing method used to generate the through-holes, a constant cross section, and axes parallel to the surface were not achieved. No other naturally occurring "defects" were obvious from analysis of the LU data carried out, in the areas scanned.

XCT

To check that no naturally occurring defects were in fact present, the samples were analysed using x-ray computed tomography (XCT) and a comparison with the LU results then made. A Nikon XT H 225 ST was used to take 1600 shots with approximately 10.6 μm voxel size. Settings of 186 kV, 220 μA, copper 1 mm filter and 0.08 exposure were selected, resulting in a scan time of 30 min. The scans were reconstructed using 'Volume Graphics' software for interrogation. Following manual alignment, a region of interest was created for the top 3 mm (z-direction) of the sample and the automated defect recognition (ADR) algorithm run to identify any voids present. Thresholds were applied at a probability threshold 0.1 and a minimum void diameter of 0.1 mm and a total of 11 voids were identified in the region. Only two voids was identified in LU scanning line regions. One in scanning line 2, and one in scanning line 3. Both indications were of large voids, greater than 700 μm diameter but were at 2 and 2.8 mm below the surface, respectively; beyond the anticipated 1064 nm limit of detection for the LU system (Fig. 9).

Destructive

In order to validate the LU and XCT results which suggested that no naturally occurring defects were present in the LU scanning line regions, destructive evaluation was carried out. A Robo-Met.3D automated serial sectioning machine was used to generate reconstructed microscope images over the area indicated in Fig. 10.

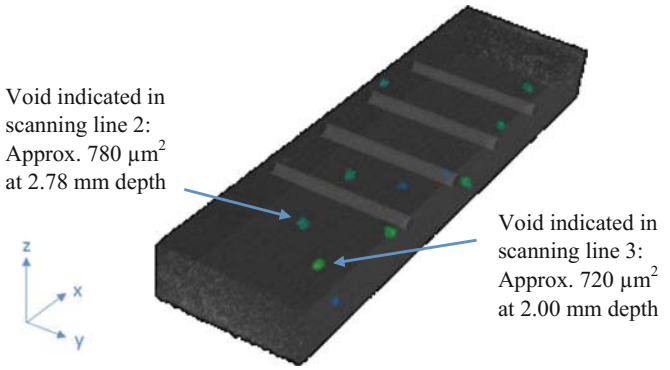

Fig. 9 Extract from 'Volume Graphics' showing voids identified in region of interest by automated defect recognition software

Fig. 10 Schematic (*left*) showing area of interest (*red*) for destructive evaluation

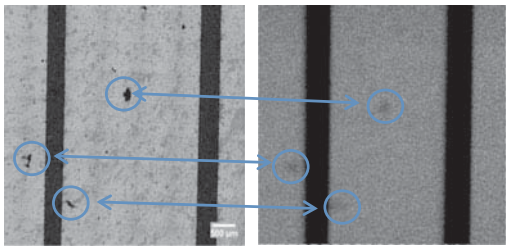

Fig. 11 Images showing good correlation between micrograph (*left*) and XCT image (*right*) at 643 µm depth

The micrograph images were compared directly with the XCT reconstructions to identify any naturally occurring defects in this area and a reasonable correlation found, albeit with poor contrast. Obvious material discontinuities identified on the micrographs were linked to indications of defects (as deviations in the greyscale) in the XCT reconstructions (Fig. 11). It can be concluded that the XCT gives a good representation of the sample integrity. However, not all of the naturally occurring defects found by destructive analysis were found by the ADR algorithm; this was probably due to the very small changes in greyscaled value. Although a time consuming activity with room for human error, it is recommended that an additional manual analysis of XCT reconstructions is carried out in future analyses.

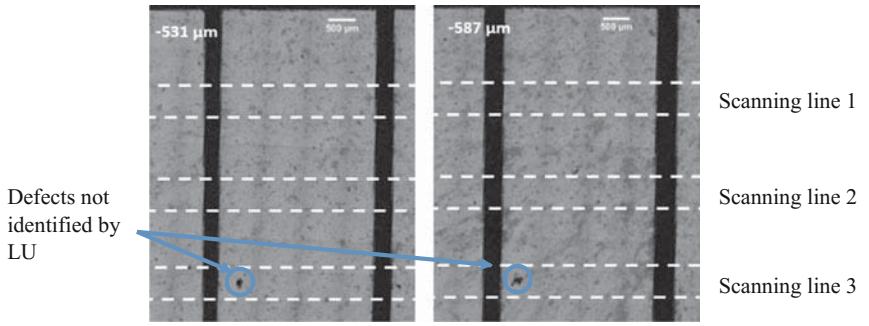

Fig. 12 Micrograph images at depths of 531 and 587 µm, showing the scanning line regions. Previously unidentified (by LU) defects are highlighted

After overlaying the LU scanning lines on the micrographs, it was found that there was one void present in the region destructively analysed, which had not been indicated from the LU B-scan (Fig. 12). The unidentified defect has dimensions of approximately 200 × 150 × 100 µm and is located 250 µm from the EDM'd "hole A" at a depth of roughly 530 µm from the top surface. For reference, "hole A" has a diameter of 580 µm and is 417 µm below the sample surface. It is thought that the presence of such a large, manufactured defect in the vicinity of the naturally occurring defect is having a masking effect.

Conclusions

Laser ultrasound has been used to identify the presence of four large (580–670 µm at 400–800 µm depth), manufactured though-holes in a Ti-6Al-4 V AM sample with an as-built surface finish. No further defects have been identified using LU. Further interrogation of the sample using XCT with ADR identified eleven possible naturally occurring defects. Two of these possible defects were located in the LU scanning line regions, although both were at a depth exceeding the anticipated capability of the LU system with current settings. No false positives were identified.

Destructive evaluation of a small region of the sample revealed a defect with dimensions of approximately 200 × 150 × 100 µm at a depth of 530 µm from the top surface, which had been 'missed' by LU and XCT ADR. It is possible that the close proximity of this naturally occurring void to the manufactured through-hole is masking any change in the Rayleigh wave arrive time in the LU signal. The greyscale settings and threshold values could be responsible for the defect not appearing with ADR. In future, manual analysis of the XCT reconstructions is recommended.

Additional work is required before it can be concluded that LU shows promise as an in-situ inspection system for AM. Multiple build layers could be assessed in a single scan, reducing the area interrogated with each build layer. The laser spot size could be altered to increase the wave penetration. Further work is required to assess the capability of the system to detect naturally occurring defects and to investigate the effect of defect density.

Acknowledgements The primary author is working within the Manufacturing Technology Engineering Doctorate Centre, supported by the Manufacturing Technology Centre, University of Nottingham and the Engineering and Physical Sciences Research Council under Award No. 1361477. Work has been carried out in conjunction with FP7-2012-NMO-ICT-FoF project 313781, AMAZE.

References

1. T.T. Wohlers, *Wohlers Report 2015*, vol. 22. Wohlers Associates (2015)
2. A.M. Uriondo, M. Esperon-Miguez, S. Perinpanayagam, The present and future of additive manufacturing in the aerospace sector: a review of important aspects, in *Proceedings of the Institution of Mechanical Engineers, Part G: Journal of Aerospace Engineering* (2015)
3. Energetics Incorporated, *Measurement science roadmap for metal-based additive manufacturing*, National Institute of Standards and Technology, Maryland, US (2013)
4. AM Steering Group UK. *UK national strategy for additive manufacturing/3D printing* (2015), http://www.amnationalstrategy.uk/steering-group/
5. I. Gibson, D.W. Rosen, B. Stucker, *Additive Manufacturing Technologies: Rapid Prototyping to Direct Digital Manufacturing* (Springer, 2009)
6. M. Van Elsen, *Complexity of Selective Laser Melting: a new optimisation approach,* PhD Thesis published, Katholieke Universiteit Leuven, Belgium (2007), pp. 31–42
7. H. Gong et al., Influence of defects on mechanical properties of Ti–6Al–4 V components produced by selective laser melting and electron beam melting. Mater. Des. **86**, 545–554 (2015)
8. S. Tammas-Williams et al., XCT analysis of the influence of melt strategies on defect population in Ti–6Al–4 V components manufactured by selective electron beam melting. Mater. Charact. **102**(4), 47–61 (2015)
9. K. Monroy, J. Delgado, J. Ciurana, Study of the pore formation on CoCrMo alloys by selective laser melting manufacturing process. Manuf. Eng. Soc. Int. Conf. MESIC Procedia Eng. **63**, 361–369 (2013)
10. C. Weingarten et al., Formation and reduction of hydrogen porosity during selective laser melting of AlSi10Mg. J. Mater. Process. Technol. **221**, 112–120 (2015)
11. W.E. King et al., Observation of keyhole-mode laser melting in laser powder-bed fusion additive manufacturing. J. Mater. Process. Technol. **214**(12), 2915–2925 (2014)
12. H. Gong et al., Defect morphology in Ti-6Al-4 V parks fabricated by selective laser melting and electron beam melting, in *Solid Freeform Fabrication Symposium*. Austin, TX (2013)
13. S.K. Everton et al., Review of in-situ process monitoring and in-situ metrology for metal additive manufacturing. Mater. Des. **95**, 431–445 (2016)
14. S.K. Everton et al., Evaluation of laser ultrasonic testing for inspection of metal additive manufacturing, in *SPIE*, San Francisco, CA, US (2015)
15. S.P Santospirito et al., Defect detection in laser powder deposition components by laser thermography and laser ultrasonic inspections in *SPIE*, San Diego, CA (2013)

16. D. Cerniglia et al., Inspection of additive-manufactured layered components. Ultrasonics **62**, 292–298 (2015)
17. R.S. Edwards et al., Scanning laser source and scanning laser detection techniques for different surface crack geometries. AIP Conf. Proc. **1430**(1), 251–258 (2012)
18. M. Klein, T. Sienicki, J. Eichenbergeer, *Laser-ultrasonic detection of subsurface defects in processed metals.* Patent. 2007: United States